ChemPubSoc Europe

DOI: 10.1002/cctc.201701667

CHEMCATCHEM Full Papers

Bifunctional Catalysis for the Conversion of Synthesis Gas to Olefins and Aromatics

J. Lennart Weber,[a] Iulian Dugulan,[b] Petra E. de Jongh,[a] and Krijn P. de Jong*[a]

The conversion of synthesis gas (a mixture of hydrogen and carbon monoxide) to value-added chemicals has attracted significant attention in the past few years. Strong emphasis has been placed on enabling a process that allows the production of short olefins from synthesis gas, which can be derived from coal, biomass, or natural gas. Here, we introduce bifunctional catalysis to tailor the selectivity towards aromatics next to olefins by combining an iron-based Fischer–Tropsch to olefins catalyst with the acid function of a zeolite. Olefins were formed from synthesis gas on an iron-based catalyst and partly converted to aromatics on the acid sites of the zeolite. Surprisingly, this aromatization did not follow the pathway of hydrogen transfer, whereby three paraffin molecules are produced for every aromatic molecule formed, which allowed us to obtain carbon selectivity towards chemicals (sum of lower olefins and aromatics) of 70–80% at 1 bar reaction pressure. Increasing the partial pressure of hydrogen led to substantial hydrogenation of olefins towards paraffins.

Introduction

In the past few years the conversion of synthesis gas to chemicals has often been aimed at the production of lower olefins from a wide range of feedstocks other than crude oil. Recent publications have shown that Fischer–Tropsch to olefins (FTO) allows the formation of lower olefins with high selectivity, using promoted iron-based and cobalt-carbide-based catalysts, which give rise to deviation from the Anderson–Schulz–Flory (ASF) distribution.[1–3] Another approach to form olefins and/or aromatics with high selectivity is the combination of a methanol synthesis catalyst with an acid function of a SAPO34 or H-ZSM-5 zeolite in a single reactor[4–8] or multiple reactors.[9,10] To extend the product spectrum of the Fischer–Tropsch synthesis, acid sites can be appended to the metal catalyst, and the proximity of those two sites can have a major effect on selectivity and activity.[4,5,11] Cobalt-catalyzed low-temperature Fischer–Tropsch synthesis provides a wide range of products from methane (C_1) to waxes (C_{20+}).[12,13] The supplement of an H-ZSM-5 zeolite facilitates cracking of the C_{12+} fraction to hydrocarbons in the gasoline range (C_5–C_{12}) with a total carbon selectivity of close to 60%.[14–16]

Combining an unpromoted iron-based FTS catalyst forming olefins with a zeolite enables the formation of aromatics to a certain degree[17,18] related to the higher reactivity of olefins compared with paraffins and the variability in reaction temperature of iron catalysts.[19–21] According to the hydrogen transfer mechanism, three paraffin molecules are produced from olefins for every aromatic molecule that is formed.[9,17,22–24] This decreases the carbon utilization towards valuable chemicals.

In this study, we will show that extending the product spectrum of the FTO process by aromatics by the combination of a promoted FTO catalyst with an H-ZSM-5 zeolite not only increases the activity of the former but also the selectivity to aromatics compared with an iron-based FTS catalyst. Furthermore, we will show the influence of reactor bed configuration and composition of synthesis gas on the catalytic performance and the product spectrum. Moreover, the formation of paraffins from olefins during aromatization was negligible and we introduce an alternative pathway for the aromatization of FTO olefins that involves dehydrogenation rather than hydrogen transfer.

Results

We prepared an unpromoted (5.6 wt% iron on alpha-alumina, Na/Fe = 0.015 at/at, denoted as Fe) and a promoted iron catalyst (5.5 wt% iron on alpha-alumina, Na/Fe = 0.144 at/at, S/Fe = 0.0093 at/at, denoted as FeP) by incipient wetness impregnation (Table S2 in the Supporting Information). The calcined iron catalysts were than combined with the pelletized H-ZSM-5 zeolite (Si/Al = 15 at/at) in different volumetric ratios of zeolite to iron catalyst in a quartz fixed-bed reactor. Here, experiments were conducted in different reactor configurations, namely mixed bed and stacked bed.

To investigate the influence of proximity of the zeolite to the iron catalysts on activity and selectivity, mixed bed experiments were conducted. All catalysts first were tested under the

[a] J. L. Weber, Prof. Dr. P. E. de Jongh, Prof. Dr. K. P. de Jong
Inorganic Chemistry and Catalysis
Debye Institute for Nanomaterials Science
Utrecht University
Universiteitsweg 99, 3584 CG, Utrecht (The Netherlands)
E-mail: k.p.dejong@uu.nl

[b] Dr. I. Dugulan
Fundamental Aspects of Materials and Energy
Radiation Science and Technology, Delft University of Technology
2629 JB, Delft (The Netherlands)

Supporting information and the ORCID identification number(s) for the author(s) of this article can be found under https://doi.org/10.1002/cctc.201701667.

reaction conditions 400 °C, 1 bar, $CO/H_2 = 1$ v/v, CO conversion < 5% to introduce a benchmark for the experiments in which the iron catalysts were mixed with the zeolite. The promoted iron catalyst (FeP) showed higher activity compared with unpromoted (Fe; Figure 1a), whereas the selectivity to methane was decreased (Figure 1c). Furthermore, the C_2–C_4 fraction (olefins and paraffins) of the promoted catalyst was higher than expected based on the limitation by the ASF distribution (maximum selectivity of C_2–C_4-fraction: 58%$_C$[1]) with 63%$_C$ (61%$_C$ olefins and 2%$_C$ paraffins). This was not the case for the unpromoted catalyst (49%$_C$ olefins and 2%$_C$ paraffins). When mixed with the zeolite in a ratio of $V_{zeolite}/V_{iron\ catalyst} = 2$ v/v as a physical mixture of the pelletized catalyst particles, the activity of the mixture of the promoted iron catalyst and the zeolite (FeP-2Z) was enhanced significantly, whereas the activity for the mixture of the unpromoted iron catalyst and the zeolite (Fe-2Z) decreased slightly (Figure 1a). In the first 15 h on stream, the selectivity towards methane of both iron catalysts was not influenced strongly by the addition of the zeolite. In the case of the promoted iron catalyst mixed with the zeolite, the total selectivity to chemicals is 68%$_C$ (51%$_C$ C_2–C_4 olefins and 17%$_C$ aromatics), whereas the promoted iron catalyst alone showed 61%$_C$ C_2–C_4 olefins without aromatics formed. The mixtures of both iron catalysts with the zeolite showed similar selectivities towards C_2–C_4 paraffins (2%$_C$ for Fe-2Z and 4%$_C$ for FeP-2Z) compared with the iron catalysts only (2%$_C$ for Fe and FeP). Figure 1b shows that the selectivity to olefins within the C_{5+} fraction decreased when the zeolite was added (from 8%$_C$ for Fe to 2%$_C$ for Fe-2Z and from 12%$_C$ for FeP to 3%$_C$ for FeP-2Z), whereas the selectivity towards paraffins in this fraction remained constant (2%$_C$ for Fe, 1%$_C$ for Fe-2Z, 3%$_C$ for FeP, and 3%$_C$ for FeP-2Z).

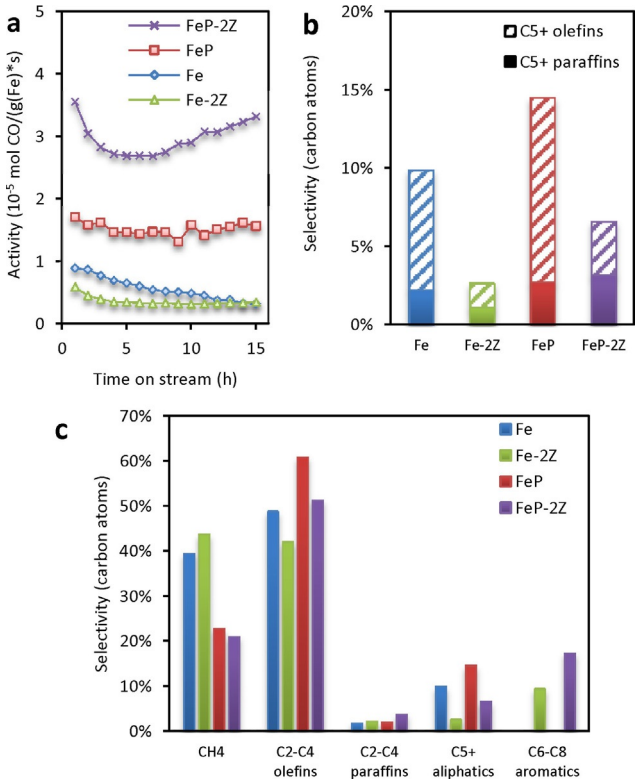

Figure 1. Activity and product distribution for the mixed-bed experiments. a) Activity during the initial phase of the reaction for the two iron catalysts with and without zeolite present in a physical mixture at 400 °C, $CO/H_2 = 1$, GHSV: 7200 h^{-1}, total pressure: 1 bar with CO conversion levels of 0.50% (Fe), 0.26% (Fe-2Z), 1.1% (FeP), and 2.0% (FeP-2Z). The addition of the zeolite has an influence on the activity of the iron catalysts. b) Distribution of olefins and paraffins within the C_{5+} fraction of mixed-bed experiments at 400 °C, $CO/H_2 = 1$, GHSV: 7200 h^{-1}, total pressure: 1 bar, and after 4 h on stream. C_{5+} olefins are also converted to aromatics. c) Carbon selectivity in the hydrocarbon products for the mixed-bed experiments at 400 °C, $CO/H_2 = 1$, GHSV: 7200 h^{-1}, total pressure: 1 bar, and after 4 h on stream. Aromatics were formed from C_2–C_4 and C_{5+} olefins.

To investigate the differences in activity of the iron catalysts when mixed with the zeolite, Mössbauer spectroscopy was performed, which is shown in Figure 2a–c. The presence of the zeolite enhanced the reduction in a more pronounced way than the presence of promoters (Figure 2b), whereas promotion showed a greater influence on the carburization (Figure 2a). After 15 h time on stream, the unpromoted iron catalyst with and without the zeolite present were not fully carburized, whereas we observed a large fraction of superparamagnetic Fe_xC (56%Fe at/at) for FeP-2Z and Hägg carbide (χ-Fe_5C_2, 67%Fe at/at) for FeP. It is not yet fully understood to what extent the different iron phases contribute to the catalytic performance.[24–26] However, it was shown that the degree of carburization has a major influence on the activity and selectivity of iron catalysts in the Fischer–Tropsch to olefins reaction.[29] Hereafter, experiments were performed in a stacked-bed configuration to exclude this influence of the zeolite on the iron carbide function.

To investigate the pathway of aromatization of olefins, the promoted iron catalyst was combined with the zeolite in a stacked-bed configuration with the zeolite downstream of the iron catalyst. The activity of the promoted iron catalyst (FeP) alone was comparable with the activity of the stacked-bed experiments (FeP-*x*Z-SB, *x* represents the ratio of zeolite to FTO catalyst, v/v), which shows that the iron catalyst is not influenced, owing to the spatial separation to the zeolite (Figure S1 in the Supporting Information). The zeolite to iron catalyst ratio was varied from $V_{zeolite}/V_{iron\ catalyst} = 2$–20 v/v (denoted as FeP-2Z-SB, FeP-10Z-SB, and FeP-20Z-SB). When combining the FTO catalyst with a low amount of zeolite in stacked-bed configuration (FeP-2Z-SB), aromatics were formed with 18%$_C$ selectivity, whereas olefins remained with 55%$_C$ selectivity (Figure 3). This gives a total selectivity to chemicals of 73%$_C$.

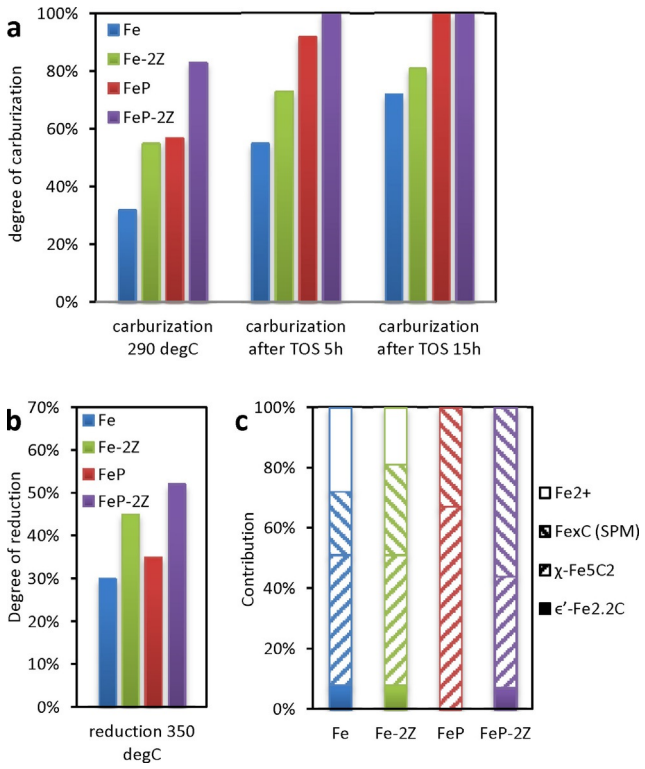

Figure 2. Degree of reduction and carburization of mixed-bed experiments. a) Degree of carburization of the two iron catalysts with and without zeolite present in a physical mixture after the in situ carburization step at 290 °C for 1 h in $CO/H_2 = 1$ with GHSV: 7200 h^{-1}, at 400 °C, $CO/H_2 = 1$, GHSV: 7200 h^{-1}, and total pressure of 1 bar after 5 h and at 400 °C, $CO/H_2 = 1$, GHSV: 7200 h^{-1}, and total pressure of 1 bar after 15 h. The presence of promoters and zeolite enhance the carburization. b) Degree of reduction of the two iron catalysts to Fe^0 with and without zeolite present in a physical mixture after in situ reduction at 350 °C for 2 h in $H_2/N_2 = 2$ with GHSV: 18000 h^{-1}, and total pressure of 1 bar. The presence of zeolite has a greater effect on the reduction than the promoters. c) Fraction of Fe^{2+} oxide and iron carbides within the total iron atoms after 15 h at 400 °C, $CO/H_2 = 1$, GHSV: 7200 h^{-1}, and total pressure of 1 bar. The presence of the zeolite has an influence on the iron carbide phases for the promoted iron catalyst. For detailed data, see Tables S3–S6 in the Supporting Information.

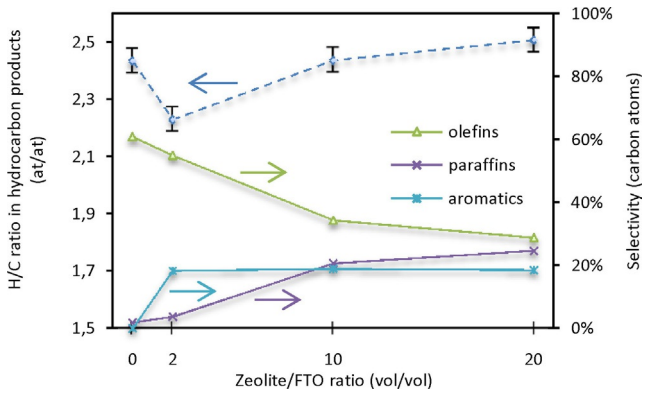

Figure 3. Atomic ratio of hydrogen and carbon in the hydrocarbon products (C_1–C_{16}) and selectivity towards olefins, paraffins, and aromatics as a function of zeolite/FTO catalyst ratio at 400 °C, $CO/H_2 = 1$, GHSV: 7200 h^{-1}, total pressure: 1 bar, and after 4 h on stream with CO conversion levels of 1.2 ± 0.1 %. The lower hydrogen/carbon ratio at zeolite/FTO of two indicates dehydrogenation. The selectivity towards aromatics stayed constant independent of the amount of zeolite added, whereas olefins were hydrogenated to form paraffins with increasing amounts of zeolite present. This resulted in an increase of the hydrogen/carbon ratio.

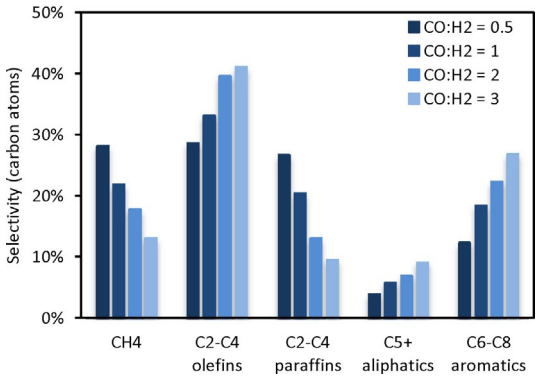

Figure 4. The product distribution of FeP-10Z-SB with variation of the feed composition from $CO/H_2 = 0.5$–3 at 400 °C, GHSV: 7200 h^{-1}, total pressure: 1 bar, and after 4 h on stream. Even though the hydrogen/carbon ratio of the hydrocarbon products at $CO/H_2 = 1$ corresponds to the ratio of the promoted iron catalysts (Figure 3), it can be seen that the selectivities of paraffins and aromatics behave in opposite manners.

Surprisingly, paraffins were formed with only 4 %$_C$ selectivity. With ascending quantity of zeolite, the selectivity towards aromatics remained constant, whereas the selectivity to olefins decreased from 55 %$_C$ to 29 %$_C$. At the same time, more paraffins were formed and the selectivity increased from 4 %$_C$ to 25 %$_C$. Increasing the amount of zeolite downstream of the FTO catalyst resulted in a decrease of selectivity to chemicals from 73 %$_C$ to 47 %$_C$. Subsequently, the composition of synthesis gas was altered from hydrogen-rich ($CO/H_2 = 0.5$) to carbon-rich ($CO/H_2 = 3$) for the FeP-10Z-SB experiment (Figure 4). Here, the methane selectivity dropped from 28 %$_C$ to 13 %$_C$, whereas olefins selectivity increased from 29 %$_C$ to 41 %$_C$. Surprisingly, the selectivities for paraffins and aromatics behaved contrary. The paraffin selectivity decreased from 27 %$_C$ to 10 %$_C$, whereas aromatics selectivity increased from 12 %$_C$ to 27 %$_C$. By raising the CO/H_2 ratio of the synthesis gas, the total selectivity to chemicals was increased from 41 %$_C$ ($CO/H_2 = 0.5$) to 68 %$_C$ ($CO/H_2 = 3$). Seemingly, the formation of paraffins and aromatics were not linked. The ratio of hydrogen and carbon of the total hydrocarbon products (C_1–C_{16}) as function of the zeolite to iron catalyst ratio shows a decrease of hydrogen content in the products for a low quantity of zeolite in respect to the FTO catalyst (Figure 3). For higher quantities of zeolite, the hydrogen/carbon ratio increased.

Discussion and Conclusion

The low selectivities towards paraffins when the iron catalysts were mixed with the zeolite implies that the pathway of aromatization of FTO olefins does not follow the hydrogen transfer pathway. According to the hydrogen transfer mechanism, lower olefins oligomerize to form olefins in the range C_6–C_{10}. Hydrogen from these longer olefins is passed on to another olefin molecule (hydrogen transfer), resulting in dienes and

paraffins. The dienes cyclize, forming cyclic olefins, which undergo two consecutive hydrogen transfer steps resulting in cyclic dienes and aromatics, respectively [Eq. (1)]. For each of these hydrogen transfer steps, one paraffin molecule is formed,[22] which would lead to a decrease in carbon utilization in terms of formation of desired chemicals (C_2–C_4 olefins and aromatics).

$$6\ C_2H_4 \rightarrow C_6H_{12} + 3\ C_2H_4 \rightarrow C_6H_6 + 3\ C_2H_6 \quad (1)$$

However, the selectivity to paraffins was surprisingly low for twice the volume of zeolite added to the iron catalysts in both mixed-bed (2.2 %$_C$ for Fe-2Z and 3.7 %$_C$ for FeP-2Z, Figure 1c) and stacked-bed configurations (3.7 %$_C$ for FeP-2Z-SB, Figure 3), whereas aromatics were formed with a substantial selectivity (9.4 %$_C$ for Fe-2Z, 17.4 %$_C$ for FeP-2Z, and 18.3 %$_C$ for FeP-2Z-SB). In the stacked-bed experiments, a lower hydrogen/carbon ratio of the hydrocarbon products was found for a zeolite/FTO ratio of two (H/C = 2.23 at/at) than the FTO catalyst without zeolite (H/C = 2.43 at/at), which suggests dehydrogenation takes place. The selectivity towards aromatics showed an independent behavior from the amount of zeolite downstream of the FTO catalyst, however, increasing the zeolite/FTO catalyst ratio led to an increase in hydrogen/carbon ratio. This increase can be attributed to the hydrogenation of olefins to paraffins with increasing zeolite/FTO ratio (Figure 3). The selectivities towards paraffins and aromatics even showed an opposite behavior when the synthesis gas composition was altered from hydrogen-rich to carbon-rich for an experiment with zeolite/FTO ratio of 10 v/v (Figure 4). This led to less extensive hydrogenation of olefins next to a shift of the equilibrium of dehydroaromatization to the side of aromatics and hydrogen (Figure S2 in the Supporting Information) and shows that the increase in hydrogen/carbon ratio in the hydrocarbon products to the initial value of the promoted iron catalyst cannot be attributed to the hydrogen transfer pathway. Therefore, we propose that the aromatization does not follow the hydrogen transfer pathway, but rather dehydroaromatization, which involves dehydrogenation instead of formation of paraffins [Eq. (2), Figure 5]. However, increasing the partial pressure of hydrogen led to more extensive hydrogenation of olefins towards paraffins [Eq. (3)]. This could be shown in experiments at 1 bar by altering the synthesis gas composition (Figure 4) as well as performing experiments at a pressure of 5 bar, where a significant fraction of olefins was hydrogenated whereas aromatics were formed with low selectivity of up to 3.1 %$_C$ (Table S7 in the Supporting Information).

$$3\ C_2H_4 \rightarrow C_6H_{12} \rightarrow C_6H_6 + 3\ H_2 \quad (2)$$

$$C_2H_4 + H_2 \rightarrow C_2H_6 \quad (3)$$

This pathway of olefin aromatization allows us to convert synthesis gas to chemicals with selectivities as high as 73 %$_C$ (55 %$_C$ lower olefins and 18 %$_C$ aromatics for FeP-2Z-SB) without giving rise to the formation of undesired paraffins at low pressure. By adjusting the reaction conditions, the fraction of aromatics within the chemicals can be altered from 25 %$_C$ (mixed bed, $CO/H_2 = 1$, zeolite/FTO = 2 v/v, 1 bar) to 40 %$_C$ (stacked bed, $CO/H_2 = 3$, zeolite/FTO = 10 v/v, 1 bar).

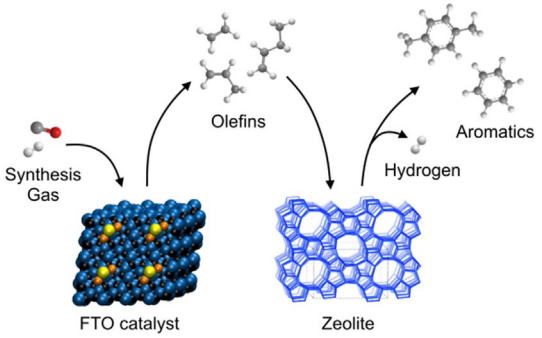

Figure 5. Proposed pathway for the conversion of synthesis gas to aromatics: Conversion of synthesis gas to olefins on the FTO catalyst, dehydroaromatization of olefins to aromatics on the zeolite.

Furthermore, the decrease in selectivity to C_2–C_4-olefins (from 61 %$_C$ for FeP to 51 %$_C$ in FeP-2Z) as well as olefins within the C_{5+} fraction (from 12 %$_C$ for FeP to 3 %$_C$ in FeP-2Z) when the zeolite was present shows that aromatics (17 %$_C$ for FeP-2Z) are not exclusively formed from C_2–C_4 olefins but also from C_{5+} olefins. Mixing the iron catalysts in close proximity with the zeolite, the catalytic activity was influenced. The activity of the unpromoted iron catalyst decreased slightly in the initial phase of the reaction, whereas the addition of zeolite to the promoted iron catalyst enhanced activity by a factor of two. This behavior can be attributed to the degree of reduction and carburization of the iron catalysts, which is influenced by the presence of the zeolite. Also, the type of iron carbide formed during activation and reaction depends on the presence of promoters[27] and zeolite and has an influence on the catalytic activity.

The addition of sodium and sulfur as promoters to an iron-based Fischer–Tropsch synthesis catalyst led to enhancement of activity and selectivity to lower olefins.[1,2,29] Now, we show that the combination of such a catalyst with a zeolite shows increased selectivity to chemicals of up to 73 %$_C$, whereas the product spectrum is extended to aromatics. Furthermore, the proximity of two functions in a bifunctional catalyst can have a significant influence on the activity and selectivity, which also applies in fields other than synthesis gas conversion.

Experimental Section

The iron catalysts were prepared by using incipient wetness impregnation of α-Al_2O_3 (BASF, AL4196E, 7 $m^2 g^{-1}$, pore volume: 0.4 $cm^3 g^{-1}$) with a solution that contains ammonium ferric citrate ($(NH_4)_xFe_yC_6H_5O_7$, 34.880 g) per 100 mL for the unpromoted iron catalyst and ammonium ferric citrate ($(NH_4)_xFe_yC_6H_5O_7$, 34.880 g), ammonium sulfate ($(NH_4)_2SO_4$, 0.165 g), and trisodium citrate dihydrate ($Na_3C_6H_5O_7 \cdot 2H_2O$, 1.225 g) per 100 mL for the promoted iron catalyst. The support was dried under vacuum at 120 °C for 2 h. Three impregnation steps were necessary to achieve an iron loading of 5.5 wt%. The subsequent calcination was performed at 250 °C for 4 h in static air. Inductively coupled plasma (ICP) analysis showed an iron loading for the unpromoted catalyst of 5.60 wt%

with a Na/Fe ratio of 0.015 at/at, owing to impurities in the iron precursor, whereas the promoted iron catalyst featured an iron loading of 5.51 wt% with Na/Fe ratio of 0.144 at/at and S/Fe ratio of 0.0093 at/at (Table S2 in the Supporting Information). The calcined catalysts were pelletized, ground, and sieved to a fraction of 75–150 μm. The iron particle sizes of the calcined catalysts were measured by transmission electron microscopy (TEM, Figure S3 in the Supporting Information), which showed an average iron oxide particle size of 10 nm, whereas FeP displayed 14 nm iron oxide particles after calcination. To determine the crystal phase of the catalysts, X-ray diffraction (XRD) patterns (Figure S4 in the Supporting Information) were recorded with a Bruker D2 Phaser powder diffractometer (CoK_α source: 1.79 Å). After calcination at 250 °C, the crystal structure of both Fe and FeP was maghemite (γ-Fe_2O_3). To transform the commercial zeolite (NH_4-ZSM-5, Zeolyst, Si/Al ratio: 15) from the ammonium form to the proton form, calcination was performed at 500 °C for 4 h in static air. Ammonium temperature-programmed desorption (TPD) data are shown in Figure S5 in the Supporting Information. Afterwards, the zeolite was pelletized, ground, and sieved to a fraction of 75–150 μm. The iron catalysts were either mixed with the zeolite in a mixed bed or placed in a stacked-bed configuration with the zeolite downstream of the iron catalyst. The catalyst bed was diluted with silicon carbide in a volume ratio of $V_{SiC}/V_{total\,catalyst} = 2$ to avoid heat transfer limitation phenomena. Prior to being subjected to the reaction conditions, the iron catalysts were reduced in situ in a stream of hydrogen and nitrogen ($H_2/N_2 = 2$ v/v, GHSV = 18000 h^{-1}, gas hourly space velocity (GHSV) was always normalized for the volume of the iron catalyst only) at 350 °C for 2 h, in which the space velocity is based on the volume flow per volume of iron catalyst. A consecutive carburization was performed at 290 °C in a stream of synthesis gas ($CO/H_2 = 1$, 1 bar, GHSV = 7200 h^{-1}) for 1 h. The catalytic testing was performed at 400 °C in a stream of synthesis gas with a GHSV of 7200 h^{-1} at ambient pressure, in which the CO/H_2 ratio of the synthesis gas was varied between $CO/H_2 = 0.5$ and 3. The CO conversion was kept below $X(CO) = 5$%. The products were analyzed with an online gas chromatograph (GC) equipped with a flame ionization detector (FID). The activity was determined based on iron time yield (FTY), which represents CO converted to hydrocarbons per second and gram of iron. Selectivities were calculated on the basis of carbon atoms within hydrocarbons formed (CO_2 free). CO conversions in the low pressure experiments were based on CO converted to hydrocarbons (CO_2 free). The selectivity to CO_2 is expected to be according to the thermodynamic equilibrium of CO, H_2, H_2O, and CO_2 in the water-gas shift reaction ($S(CO_2) \approx 47\%_C$). Experiments at elevated pressure were performed in a Avantium Flowrence 16-port parallel fixed-bed reactor setup. Prior to being exposed to the reaction conditions, the iron catalysts were reduced in situ in a stream of 30 $\%_{vol}$ hydrogen in helium (GHSV = 15000 h^{-1}) at 350 °C for 2 h at 3 bar. A consecutive carburization was performed at 290 °C in a stream of synthesis gas ($CO/H_2 = 1$, 3 bar, GHSV = 28000 h^{-1}) for 1 h. The catalytic testing was performed at 400 °C in a stream of synthesis gas with a GHSV of 24000 h^{-1} at a pressure of 5 bar, where the CO/H_2 ratio of the synthesis gas was varied between $CO/H_2 = 0.5$ and 2. The products were analyzed with an online gas chromatograph (GC) equipped with a flame ionization detector (FID) and thermal conductivity detector (TCD). The activity was determined based on iron time yield (FTY), which represents CO converted to hydrocarbons per second and gram of iron. Selectivities towards hydrocarbon products were calculated on the basis of carbon atoms within hydrocarbons formed (CO_2 free). Transmission ^{57}Fe Mössbauer absorption spectra were collected in situ at 300 K with a conventional constant-acceleration spectrometer using a ^{57}Co(Rh) source. Velocity calibration was performed by using an α-Fe foil.

Acknowledgments

This work was supported by the Netherlands Center for Multiscale Catalytic Energy Conversion (MCEC), an NWO Gravitation program funded by the Ministry of Education, Culture and Science of the government of the Netherlands. K.P.d.J. acknowledges the European Research Council, EU FP7 ERC Advanced Grant no. 338846.

Conflict of interest

The authors declare no conflict of interest.

Keywords: bifunctional catalysis · dehydrogenation · Fischer–Tropsch to olefins · synthesis gas to chemicals · zeolites

[1] H. M. Torres Galvis, J. H. Bitter, C. B. Khare, M. Ruitenbeek, A. I. Dugulan, K. P. de Jong, *Science* **2012**, *335*, 835–838.
[2] H. M. Torres Galvis, J. H. Bitter, T. Davidian, M. Ruitenbeek, A. I. Dugulan, K. P. de Jong, *J. Am. Chem. Soc.* **2012**, *134*, 16207–16215.
[3] L. Zhong, F. Yu, Y. An, Y. Zhao, Y. Sun, Z. Li, T. Lin, Y. Lin, X. Qi, Y. Dai, L. Gu, J. Hu, Q. Shen, H. Wang, *Nature* **2016**, *538*, 84–87.
[4] F. Jiao, J. Li, X. Pan, J. Xiao, H. Li, H. Ma, M. Wei, Y. Pan, Z. Zhou, M. Li, S. Miao, J. Li, Y. Zhu, D. Xiao, T. He, J. Yang, F. Qi, Q. Fu, X. Bao, *Science* **2016**, *351*, 1065–1068.
[5] K. Cheng, B. Gu, X. Liu, J. Kang, Q. Zhang, Y. Wang, *Angew. Chem. Int. Ed.* **2016**, *55*, 4725–4728; *Angew. Chem.* **2016**, *128*, 4803–4806.
[6] U. Olsbye, *Angew. Chem. Int. Ed.* **2016**, *55*, 7294–7295; *Angew. Chem.* **2016**, *128*, 7412–7414.
[7] K. Cheng, W. Zhou, J. Kang, S. He, S. Shi, Q. Zhang, Y. Pan, W. Wen, Y. Wang, *Chem* **2017**, *3*, 334–347.
[8] B. Zhao, P. Zhai, P. Wang, J. Li, T. Li, M. Peng, M. Zhao, G. Hu, Y. Yang, Y. W. Li, Q. Zhang, W. Fan, D. Ma, *Chem* **2017**, *3*, 323–333.
[9] M. Bjørgen, U. Olsbye, D. Petersen, S. Kolboe, *J. Catal.* **2004**, *221*, 1–10.
[10] U. Olsbye, S. Svelle, M. Bjørgen, P. Beato, T. V. W. Janssens, F. Joensen, S. Bordiga, K. P. Lillerud, *Angew. Chem. Int. Ed.* **2012**, *51*, 5810–5831; *Angew. Chem.* **2012**, *124*, 5910–5933.
[11] J. Zecevic, G. Vanbutsele, K. P. de Jong, A. Martens, *Nature* **2015**, *528*, 245–254.
[12] F. Fischer, H. Tropsch, *Ber. Dtsch. Chem. Ges.* **1926**, *59*, 832–836.
[13] M. E. Dry, *Catal. Lett.* **1990**, *7*, 241–251.
[14] S. Sartipi, J. E. van Dijk, J. Gascon, F. Kapteijn, *Appl. Catal. A* **2013**, *456*, 11–22.
[15] S. Sartipi, K. Parashar, M. Makkee, J. Gascon, F. Kapteijn, *Catal. Sci. Technol.* **2013**, *3*, 572–575.
[16] Q. Lin, Q. Zhang, G. Yang, Q. Chen, J. Ki, Q. Wei, Y. Tan, H. Wan, N. Tsubaki, *J. Catal.* **2016**, *344*, 378–388.
[17] A. V. Karre, A. Kababji, E. L. Kugler, D. B. Dadyburjor, *Catal. Today* **2012**, *198*, 280–288.
[18] A. V. Karre, A. Kababji, E. L. Kugler, D. B. Dadyburjor, *Catal. Today* **2013**, *214*, 82–89.
[19] I. Nakamura, K. Fujimoto, *Catal. Today* **1996**, *31*, 335–344.
[20] M. Janardanarao, *Ind. Eng. Chem. Res.* **1990**, *29*, 1735–1753.
[21] Y. Song, X. Zhu, S. Xie, Q. Wang, L. Xu, *Catal. Lett.* **2004**, *97*, 31–36.
[22] R. J. Quann, L. A. Green, S. A. Tabak, F. J. Krambeck, *Ind. Eng. Chem. Res.* **1988**, *27*, 565–570.
[23] S. Müller, Y. Liu, F. M. Kirchberger, M. Tonigold, M. Sanchez-Sanchez, J. A. Lercher, *J. Am. Chem. Soc.* **2016**, *138*, 15994–16003.
[24] D. B. Lukyanov, N. S. Gnep, M. R. Guisnet, *Ind. Eng. Chem. Res.* **1994**, *33*, 223–234.
[25] O. P. Keipert, M. Baerns, *Stud. Surf. Sci. Catal.* **1994**, *84*, 1757–1764.

[26] M. E. Dry, in *Catalysis-Science and Technology, Vol. 1* (Eds.: J. R. Anderson, M. Boudart), Springer, New York, **1981**, pp. 160 – 255.
[27] D. B. Bukur, L. Nowicki, R. K. Manne, X. Lang, *J. Catal.* **1995**, *155*, 366 – 375.
[28] M. D. Shroff, D. S. Kalakkad, K. E. Coulter, S. D. Kohler, M. S. Harrington, N. B. Jackson, A. G. Sault, A. K. Datye, *J. Catal.* **1995**, *156*, 185 – 207.
[29] J. Xie, H. M. Torres Galvis, A. C. J. Koeken, A. Kirilin, A. J. Dugulan, M. Ruitenbeek, K. P. de Jong, *ACS Catal.* **2016**, *6*, 4017 – 4024.

Manuscript received: October 18, 2017
Accepted manuscript online: October 26, 2017
Version of record online: January 26, 2018